Ver. 1.1

Handbook of optoelectronic analysis of light-emitting materials and devices

MinJae Kim
Department of Materials Science and Engineering
Korea Advanced Institute of Science and Technology

Handbook of optoelectronic analysis of light-emitting materials and devices

Handbook of optoelectronic analysis of light-emitting materials and devices

MinJae Kim

Preface

Science is all about proving your innocence. A hypothesis becomes a theory only if all the other sound alternate hypotheses are rationally rejected with sufficient evidence. A well-founded theory shall explain related observations in a reasonable manner and lucidly predict the results of an inchoate idea and to-be-performed experiments.

This book is the finishing-up of my studies, methodologies, theoretical backgrounds, and experiences in the field of crystalline light-emitting materials and devices. Leading through the following chapters, you will encounter a plethora of related disciplines, spanning from classical thermodynamics, through light-matter interactions, to basic semiconductor electronics. Albeit it cannot cover the whole physical background of optoelectronics study, because the discipline is like an assorted gift set, I sincerely hope this book helps you compose a versatile toolkit and 'prove your innocence' in your future studies.

This would not have been possible without my advisors. First and foremost, my gratitude goes to Prof. Himchan Cho who allowed me to have wonderful times and make invaluable networks in the lab. His munificent support enabled my steadfast challenges and taught me to seek *veritas*. It was a true fortune for me to have him as my advisor. I could get indispensable knowledge and insights from the teachings of Prof. Seunghyup Yoo. I was awed a lot by the dazzling intellectual sparkles of him. He and his lecture *per se* are pellucid evidence showing that merely 'reading books' is not sufficient and one must go to the classroom to truly understand and acquire. I truly enjoyed the intellectual enlightenment triggered by

Prof. Yoo. Last but not least, some parts of this book are indebted to the teachings of Prof. Mooseok Jang.
Despite the teachings of the renowned and admirable mentors, this manuscript may contain some errors or misleadings solely owing to the inadequacy of my learning and experience. If you have any ideas or opinions, please contact me *via* my homepage or email.

Dec. 2023

MinJae Kim

Table of Contents

List of Figures

CHAPTER 1

Basic understanding of the crystallization of multi-component system

Before directly delving into an optoelectronic analysis of light-emitting materials, you should get acquainted with how layers of an optoelectronic device are fabricated. In this chapter, you will learn novice physics related to spin-coating, nucleation, and growth of polymer and polycrystalline thin films. This chapter is written assuming you are given basic knowledge of Newtonian fluid dynamics and rudimentary thermodynamics. (An undergraduate-level understanding of thermodynamics would be sufficient) This chapter will be the founding basis of the later discussions and therefore you should focus on thoroughly understanding the details of this chapter.

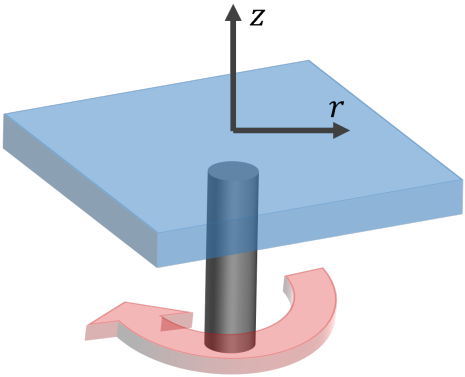

Fig. 1.1. Spin-coating system

1.1. Spin-coating process

In tandem with its facile bandgap modulation by halide alloying, solution processability is another major advantage of perovskite optoelectronics. Not only perovskite layer but also polymer layers for effective charge (typically hole injection in the case of bottom-emission devices) are fabricated by the spin-coating method as such. Therefore, you may have to understand the underlying physics of the classical spin-coating process.

Considering the nature of the process, it should be apparent to opt for the cylindrical coordinate system. Say the solution is not diffusion-limited so that concentration function $C(r,\ z,\ t)$ is independent of z and the solvent evaporation rate remains constant throughout the whole process. (for the mixed solvent system, see section 1.4.2) Also, provided the total volume of the solution is the

mere sum of that of solute (S) and solvent (L), such that $C(r,\ t) = \frac{S}{h} = \frac{S}{S+L}$. Then, for the radial flow of a Newtonian fluid q, kinematic viscosity ν, and constant evaporation rate e,

$$\begin{aligned} \frac{d}{dt}S &= -\frac{C}{r}\frac{\partial}{\partial r}(rq) = -C\frac{2\omega^2 h^3}{3\nu} \\ \frac{d}{dt}L &= -(1-C)\frac{2\omega^2 h^3}{3\nu} - e \end{aligned} \tag{1.1}$$

The critical film thickness h_0, at which the thinning mechanism is converted from the centrifugal flow to the evaporation of the solvent, is given by, from equation 1.1,

$$h_0 = \left(\frac{3\nu e}{2(1-C)\omega^2}\right)^{1/3}$$

If the airflow above the spin-coating substrate remains laminar flow, the final thickness is given by

$$h_f = \left(\frac{3K\nu C_0^3}{2(1-C_0)}\right)\frac{1}{\omega^{1/2}}$$

The relationships derived from equation 1.1 is called the Meyerhofer model. Yet the proportionality factor may differ, many experimental results revealed the validity of $\omega^{-1/2}$-dependence of the film thickness. Unless any other interruption (*e.g.* antisolvent dripping), the thickness tends to follow the rule. For example, PEDOT:PSS dispersion solution is well known to follow the relationship.

1.2. La Mer theory

Given the rudimentary understanding of spin-coating physics, we next delve into the La Mer theory. The theory, in a few words, is the bridge for the gap between the initial input and kinetics. Starting from thermodynamics, you will learn how the kinetics are related to the initial conditions of a system. Throughout this section, you should keep that the theory is based on chemical equilibrium, which may not be true in real-life processes in mind.

1.2.1 Classical nucleation theory

Consider a particle solidification from a single-component solution. Assume that the solution shows an ideal behavior and the particle is a pure single-component solid. Then, the chemical potential of the solute in liquid and solid phase are given by the following equations, respectively.

$$\mu_{M,l} = \mu^{\circ}_{M,l} + kT \ln a_{M,l} = \mu^{\circ}_{M,l} + kT \ln X_{M,l}$$
$$\mu_{M,s} = \mu^{\circ}_{M,s}$$

At equilibrium, $\mu_{M,l} = \mu_{M,s}$ so that the following holds.

$$\mu^{\circ}_{M,l} - \mu^{\circ}_{M,s} = -kT \ln X^{eq}_{M,l}$$

Then the Gibbs free energy change of the phase transformation accordingly would be:

$$\begin{aligned}\Delta G_v &= \mu_{M,s} - \mu_{M,l} \\ &= \mu^{\circ}_{M,s} - (\mu^{\circ}_{M,l} + kT \ln X_{M,l}) \\ &= -kT \ln \left(\frac{X_{M,l}}{X^{eq}_{M,l}} \right) \\ &\equiv -kT \ln \left(\frac{C}{C_0} \right)\end{aligned}$$

For the absolute supersaturation $\alpha \equiv \frac{C-C_0}{C_0}$ and molar volume Ω, molar phase transformation energy would be:

$$\Delta \mu_v = -\frac{kT}{\Omega} \ln (1+\alpha) \tag{1.2}$$

The total free energy is contributed by (1) phase transformation ($\Delta \mu_v$) and (2) interface formation ($\Delta \mu_s$). Therefore, the total change of chemical potential owing to the formation of a spherical nucleus is given by:

$$\Delta G = \Delta \mu_v + \Delta \mu_s = \frac{4}{3} \pi r^3 \Delta G_v + 4\pi r^2 \gamma \tag{1.3}$$

Because $\mu_v < 0$ and $\mu_s > 0$ for $\alpha > 0$, the $\Delta G(r)$ has the global maxima at a certain finite radius r_c (critical radius) such that $\frac{d}{dr} \Delta G(r)|_{r<r_c} > 0$ and $\frac{d}{dr} \Delta G(r)|_{r>r_c} < 0$. Mathematically, $\frac{d}{dr} G(r)|_{r=r_c} = 0$ and consequently,

$$\begin{aligned} r_c &= -\frac{2\gamma}{\Delta G_v} \\ \Delta G_c &= \frac{16\pi\gamma^3}{3(\Delta G_v)^2} \end{aligned} \tag{1.4}$$

For heterogeneous nucleation, in which a nucleus is formed at the interface between the liquid and existing substrate, the r_c and ΔG_c are scaled by a geometric factor $S(\theta)$, where θ is the contact angle between the solid and the substrate. For spherical geometry, $S(\theta) = \frac{1}{4}(2+\cos\theta)(1-\cos\theta)^2 \leq 1$. Therefore, the critical radius (the minimal radius of a nucleus not to dissolve spontaneously) is smaller for the heterogeneous nucleation compared to the homogeneous one.

1.2.2 La Mer diagram

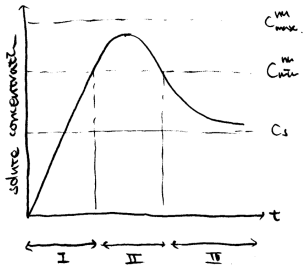

Fig. 1.2. La Mer diagram

La Mer diagram is a visualization of solute concentration as a function of time in the classical nucleation-growth process. In figure 1.2, C_s is the equilibrium concentration of the solute ($= C_0$), and C_{min} is the supersaturated concentration required to overcome the critical Gibbs free energy barrier for nucleation, ΔG_c. According to the La Mer theory, a nanoparticle synthesis process is comprised of the following three regimes.

1. Rapid increase in the concentration of free monomer in solution
2. Burst nucleation and a significant decrease in free monomer concentration
3. Growth of nanoparticles under the control of diffusion

The three regimes are respectively indicated in figure 1.2 with I, II, and III. The first step is typically done by antisolvent dripping in the case of quasi-2D perovskite synthesis. As also can be deduced intuitively, the higher the monomer concentration the initial solution has, the smaller nanoparticles with narrower size distribution are formed. Yet it is still controversial if the La Mer theory can duly describe multi-component crystallization, it is apparent that it cannot directly describe the final size distribution.

1.3. Wiemarn's theory

With the given advantages and drawbacks of the La Mer diagram in mind, Wiemarn's theory could be an excellent alternative to the La Mer theory. Especially, it is imperative to describe an ensemble of anisotropic nanomaterials, which cannot be described with the La Mer theory in a simple manner. Wiemarn's theory is about thermodynamics and consequently describes the final product as a state function of initial conditions. Contrary, the La Mer theory has something to do with kinetics and accordingly bears path function nature. The input of Wiemarn's theory is the supersaturation of solute, $\sigma(T)$, and the output is crystallite size. The theory describes the following two things:

- How supersaturation $\sigma(T)$ is related to process rates.
- How crystallite size depends on each process rate.

To this end, the theory aims to reveal the connection between supersaturation $\sigma(T)$ and crystallite size $S(\sigma)$. In general, nucle-

ation rate $V_1(\sigma)$ and growth rate $V_2(\sigma)$ are given as follows:

$$V_1(\sigma) = A_1 \exp\left(-\frac{1}{\sigma^2}\right)$$
$$V_2(\sigma) = A_2\sigma^2 \tanh\left(\frac{B}{\sigma}\right)$$

As intuitively deduced from the equations above, both V_1 and V_2 are monotonic increasing functions of σ. Moreover, increasing rate $\frac{d}{d\sigma}V_j(\sigma)$ goes larger for a concentrated solution.

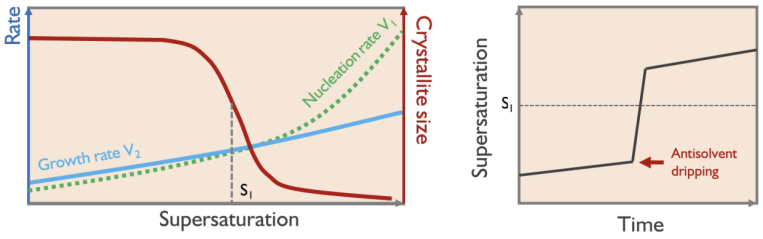

Fig. 1.3. Wiemarn's theory

Figure 1.3 illustrates typical rates of growth and nucleation behavior anticipated by Wiemarn's theory. As one can easily anticipate, the crystallite size would be proportional to V_2/V_1. At a low-σ regime, in which the growth rate exceeds the nucleation rate (*i.e.* $V_2(\sigma) > V_1(\sigma)$), crystallite size remains large and relatively unchanged. At a high-σ regime, contrastingly, crystallite size remains small because nucleation outperforms growth kinetics.
The true value of this theory is its versatility. It is widely known that the description is valid for multi-component systems and moreover, for a plethora of form factors spanning from quantum dot

synthesis to polycrystalline thin film. Quasi-2D perovskite thin film fabrication, for example, could be simply represented by a $\sigma - t$ graph of figure 1.3. During a spin-coating process, supersaturation naturally grows owing to the gradual evaporation of the solvent. At the juncture of antisolvent drips onto the film, it would jump σ abruptly because it contributes to solubility negatively, removes residual solvents, and evaporates volatile. Therefore, high supersaturation is imperative to yield quasi-2D perovskite film with small $\langle n \rangle$.

1.4. Crystallization theory of quasi-2D perovskite at a glance

With the proven track of the versatility of the model, combined with reproduced experimental results, the S^3 model is proposed here.

Initially, the lead bromide polyhedral component, A-site ion, and spacer molecule are solvated by solvent molecule, DMSO in figure 1.4. Upon antisolvent dripping, partial removal of the solvent molecule results in desolvation and consequently, it proceeds to nucleus formation or takes an excursion to form other phases, 1D perovskite for example. Presumably, the demarcation concentration of the intermediate for the formation of a nucleus is higher than that for the excursion. As long as the nucleus is formed, it undergoes subsequent growth, the rate of which is mainly determined by Wiemarn's theory.

The below two insets of figure 1.4 are the photoluminescence and absorption spectra respectively for the film fabricated by two precursor solutions, with one concentration being double the other. As expected by Wiemarn's theory, higher solute concentration results

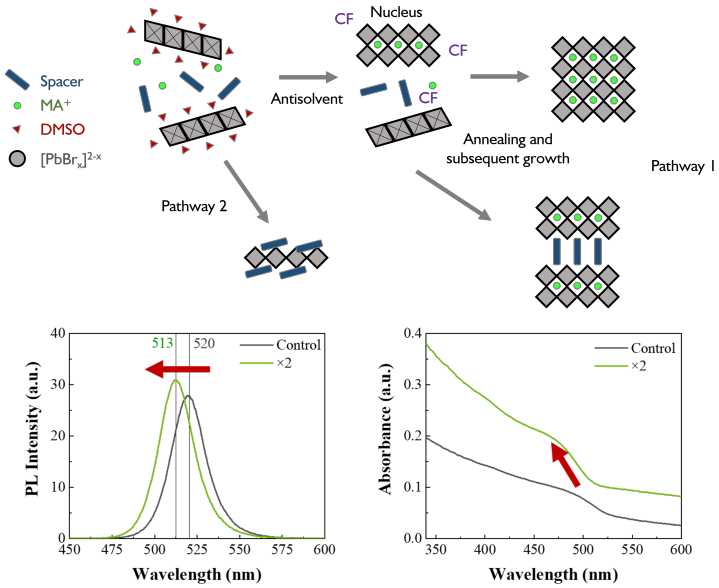

Fig. 1.4. S^3 model

in low $\langle n \rangle$ and blueshifted optical properties, consequently. Moreover, raising the supersaturation level also results in suppressed excursion. Here, one should note that, depending on the chemical nature of the spacer molecule, one may omit pathway 2.

1.4.1 Solute concentration effect

The experimental results shown in figure 1.4 not only validate the S^3 model but also denote one shall not opt to simply concentrate the precursor solution just to thicken the film. Contrary to typical

organic polymer films, the thickness of which is directly proportional to solution concentration with all the other factors are identical, perovskite films with rich precursor solution have different thicknesses, phase distributions (hence emission wavelength), and even compositions. What is more, the thickness does not have a linear relationship with the concentration owing to viscosity and antisolvent dripping-dependent fluid dynamics. Therefore, one should refrain from being seduced by 'intuition to thicken the solution.'

1.4.2 Antisolvent doping

Figure 1.4 likewise signifies that solution and antisolvent composition also play a critical role in polycrystalline perovskite thin film fabrication. For example, one can 'dope' a small amount of antisolvent to precursor solution to boost its supersaturation α. As shown in figure 1.5, photoluminescence peak wavelength underwent blueshift with an ascending amount of antisolvent added. Surprisingly, antisolvent dripping time-dependence of photoluminescence peak shift showed an opposite propensity between doped and undoped systems. Contrary to the former case, in which delayed antisolvent dripping resulted in bathochromic change, the latter case showed a clear blueshift.
The results from the undoped solvent system are straightforward. As expected from Wiemarn's theory, (see Section 1.3) temporal evaporation of solvent would lead the solution to have a higher starting point prior to antisolvent dripping and hence resulted in higher α throughout the crystallization process, which ultimately renders grains smaller. The striking point here is the redshift in

the antisolvent-doped case. It implies that there exists a temporal regime in which $\frac{\partial}{\partial t}\sigma < 0$. With this observation, you may clearly envisage the abstract shape of $\sigma(t)$ as shown in figure 1.5.

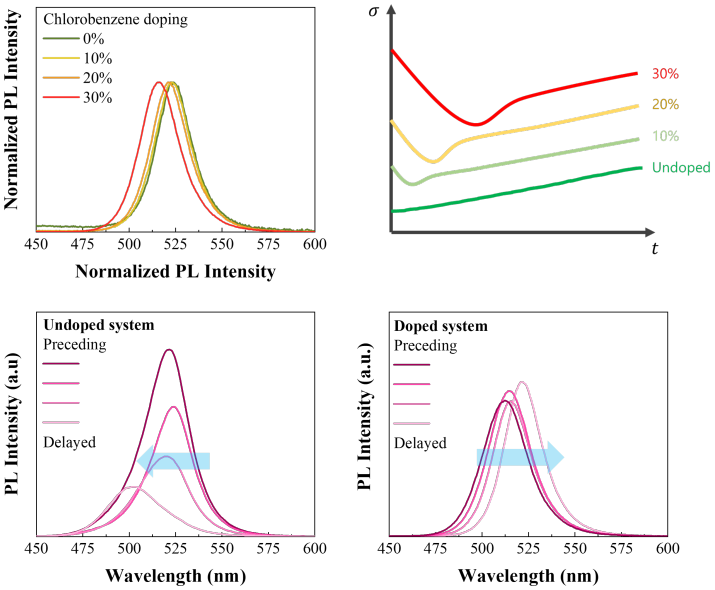

Fig. 1.5. Antisolvent doping effect

The presumed $\sigma(t)$ is also consistent with the results anticipated by the simple model. For the system in a non-equilibrium state, evaporation rates can be utilized to describe the composition of the solvent. For the sake of succinct description, the initial total volume of the system is set to be 1. To formalize in a general manner, define the initial composition, evaporation rate, and solubility

of the solute as χ_i, η_i, and β_i, respectively. Also, set the initial solute dissolved in the multinary solvent system as α. Then, one can write the total volume as a function of time as follows:

$$\begin{aligned} V(t) &= \sum_i \chi_i (1 - \eta_i t) \\ &= 1 - t \sum_i \chi_i \eta_i \end{aligned}$$

Consequently, the concentration of the solute as a function can be described as (note that $\sum \chi_i = 1$ by definition)

$$C(t) = \frac{\zeta}{1 - t \sum_i \chi_i \eta_i}$$

Then, for time t, the solubility of the solute can be described as:

$$C_{eq}(t) = \frac{\sum_i \chi_i \beta_i (1 - \eta_i t)}{1 - t \sum_i \chi_i \eta_i}$$

Hence, the supersaturation as a function of time is written as:

$$\begin{aligned} \sigma(t) &= \frac{C}{C_{eq}} \\ &= \frac{\zeta}{\sum_i \chi_i \beta_i (1 - \eta_i t)} \end{aligned} \tag{1.5}$$

A cerebral person may easily get equation 1.5 is consistent with the graphs in figure 1.5, which is intuitively derived from the experimental results.

The antisolvent doping reverses the trend of time-dependent supersaturation level change. In the undoped case, $\partial \sigma / \partial t$ remains to be

positive throughout the process. Contrastingly, when it comes to an antisolvent-doped system, $\partial\sigma/\partial t$ becomes negative in the initial stage. Therefore, in that particular regime, the propensity of antisolvent dripping time-dependent physical behaviors would be reversed. As a prominent example, the morphology (hence leakage current in the electroluminescence devices) could be enhanced even in preceding antisolvent dripping, while a smooth surface could be achieved only by delayed antisolvent dripping, which aggravates the photoluminescence quantum yield of a quasi-2D perovskite film, in the undoped system. This technique was devised and coined as the 'antisolvent addition reverses critical trade-offs by inversion of the curve' (AntARCTIC) method by the author.

CHAPTER 2

Quantum mechanical description of optical processes

Optoelectronics is all about light-matter interaction. Light, an electromagnetic wave, is the product of the momentum change of a charged actor. In this section, however, the light is treated as the product of dipole moment change keeping the optoelectronic applications in mind. Some parts of this chapter are described in a quasi-classical manner to further enhance the intuitive understanding of basic optoelectronic processes. If you are not familiar with some important concepts in solid-state physics including Bloch theorem, Fermi-Dirac and Maxwell-Boltzmann statistics, Hilbert space, and related disciplines, you may have to recall your basic understandings. Through studying this chapter, you can get a basic yet versatile toolkit to understand the later part of this book.

2.1. Exciton

2.1.1 Effective mass model

'An electron and a hole weakly bound with Coulomb force'. This is a very well-known, typical, and tedious explanation of an exciton. Under such an explanation, an exciton is modeled by the hydrogen atom model. Consequently, the potential function would be given by Coulomb potential so that

$$V(r) = -\frac{1}{4\pi\varepsilon_0}\frac{e^2}{r}$$

Then the total eigenvalue equation would be

$$\left(-\frac{\hbar^2}{2m}\nabla^2 + V\right)\psi = E\psi$$

It is rather simple but tedious to solve the differential equation, so here we directly dive into the results. (Nevertheless, try to solve the equation in the spherical coordinate system to reminisce your undergraduate studies.) The eigenvalue of the equation is given by

$$E_n = -\frac{\mu e^4}{32\pi^2\varepsilon^2\hbar^2}\frac{1}{n^2}$$

Because it is the 'binding energy' of an exciton, the total energy of an exciton is given by

$$E_n' = E_g + E_n \tag{2.1}$$

The energy eigenvalue E_n reduces the effective gap and defines the 'optical bandgap.' (E_n')

2.1.2 Bloch description

Understanding the band structure for an exciton is the foremost priority in studying optoelectronic devices. Yet we have dealt with the effective mass model, (section 2.1.1) it was based on the 'spherically symmetric potential field' assumption, which is not true in real cases. To cope with the potential error, consider a ring crystal with N atoms (spaced by a) with the ground state articulated by u_j. Then, the ground state of the whole system is described as

$$\psi_g = \prod_{i=1}^{N} u_i$$

If the jth atom is promoted to the excited state, v_j, the total wavefunction will become

$$\psi_{u,j} = \left(\prod_{i=1}^{j-1} u_i \right) v_j \left(\prod_{i=j+1}^{N} u_i \right)$$

Then the total eigenvalue equation is given by

$$\mathscr{H}\psi_{u,j} = \varepsilon\psi_{u,j} + T\left(\psi_{u,j-1} + \psi_{u,j+1}\right)$$

where T indicates the interaction between the adjacent excited states. It is apparent that the above equation would have the Bloch-wavefunction such that

$$\psi_{u,k} = \sum_j \exp(ijka)\psi_g$$

As such, the eigenvalue corresponding to the Bloch-type eigenfunction would be

$$\begin{aligned}\mathscr{H}\psi_{u,k} &= \sum_j \exp(ijka)\mathscr{H}\psi_g \\ &= \sum_j (\varepsilon + T(\exp(ika)+\exp(ika)))\exp(ijka)\psi_g \\ &= (\varepsilon + 2T\cos(ka))\psi_{u,k} \\ E_k &= \varepsilon + 2T\cos(ka)\end{aligned} \tag{2.2}$$

Consequently, a Frenkel exciton has a band structure represented by the cosine-type oscillation of energy with respect to $\vec{k}$.

2.1.3 Saha-Langmuir equation

With the given rudimentary understanding of an exciton, its separation into free carriers can be described using ionization theory. Especially, the Saha-Langmuir theory, originally has been being used in astrophysics, is adopted to model the separation of an exciton in a dynamic equilibrium. If exciton-exciton interaction is negligible (*i.g.* no wavefunction overlap), and given total excited state N in equilibrium, for the number of free electron-hole pairs and excitons of n_{eh} and e_{exc}, respectively,

$$N = n_{eh}(T) + n_{exc}(T)$$

Then the relative balance between free carriers and excitons is given by thermal equilibrium such that

$$\frac{n_{eh}^2}{n_{exc}} = \frac{\mu kT}{32\pi\varepsilon^2\hbar^2}\exp\left(-\frac{E_b'}{kT}\right)$$

where E_b' is the renormalized exciton binding energy. Consequently, the fraction of free charge carrier x is given by

$$\frac{x^2}{1-x} = \frac{1}{n}\left(\frac{32\pi\mu kT}{\hbar^2}\right)^{3/2} \exp\left(-\frac{E_b}{kT}\right) \tag{2.3}$$

where n is the excitation density.

2.2. The density of states in 2D quantum well

Consider a 2D quantum well. Regardless of the semi-infinitely long well height, whether it is infinite or definite, the allowed energy state is quantized in the normal direction. For the infinite quantum well with its width of L, the quantized wave vector is restricted to have its wavevector of integer multiples of π/L. Therefore, in k-space, the density of states is given by

$$g(k_\perp) = \left(\frac{1}{2\pi}\right)^2$$

To make it physically meaningful and versatile, it is required to be transformed from the k-space representation to the E-space. Considering the symmetry of the potential well, the infinitesimal areal part in k-space is given by $d^2k_\perp = d(\pi k_\perp^2) = 2\pi k_\perp dk_\perp$. Then, by the rudimentary calculus,

$$g(E)dE = g(k_\perp)d^2k_\perp$$

and consequently,

$$g(E) = \frac{k_\perp}{\pi}\frac{d}{dE}k_\perp \tag{2.4}$$

Because the total energy is given by (recall 2D particle-in-the-box problem!)

$$E_j = \frac{\hbar^2}{2m} k_\perp^2 + \frac{\hbar^2}{2m} \left(\frac{j\pi}{L} \right)^2$$

Therefore, equation 2.4 becomes

$$\begin{aligned} g(E) &= \frac{m}{\pi\hbar^2} \\ \text{Generally, } &= \sum_j \frac{m}{\pi\hbar^2} \mathfrak{H}(E - E_j) \end{aligned} \tag{2.5}$$

where $\mathfrak{H}(x)$ is the Heaviside step function. As such, contrary to the 3D case, the density of states is incontinuous. However, this 'perfect' 2D model cannot thoroughly explain the absorption results of so-called '2D' materials, because they do have thickness. In reality, the density of states of such 2D or quasi-2D materials exhibits something between 3D and perfect 2D.

2.2.1 Quantum-confined Stark effect

We have treated symmetric quantum wells in obtaining eigenfunctions and corresponding eigenvalues. Under an electric field, the well would be skewed and electrons and holes would be pushed to the opposite part of the well. (This is called 'field-induced ionization of an exciton') (see figure 2.1) In the case of a quantum well, however, the ionization is drastically limited by the potential barriers of the well, and hence the exciton is not separated into free carriers. Therefore, a quantum well structure retains its excitonic emission vertexes even under a strong field. (see section 3.5)

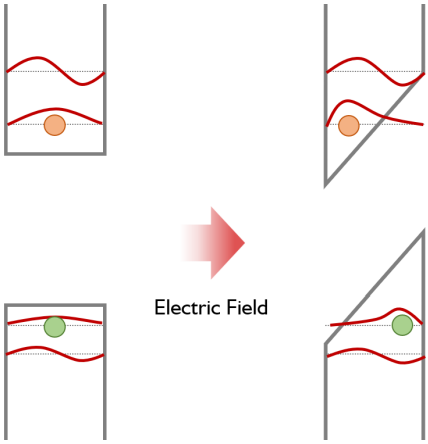

Fig. 2.1. Quantum-confined Stark effect

In tandem with the high-field survival of the exciton state, the field also broadens the potential well. This results in a discriminative redshift in both absorption and emission. In other words, every electroluminescence is bathochromic compared to its photoluminescence. The redshift could be observed in electroluminescent devices with quantum-confined nanomaterials, including quantum dots, nanorods, and nanoplatelets, as the active material.

2.2.2 Forbidden transitions allowed

The collapse of potential symmetry by external fields also ruptures the transition selection rule dictated by Fermi's Golden Rule (see section 2.3). Provided no external field, transitions with $\Delta j \neq 0$ are forbidden because the overlap integral goes to zero. However,

under the exertion of an external field, wavefunctions of electron and hole are no longer symmetrical, and the asymmetry unleashes the feasibility of the forbidden transition.

2.3. Fermi's golden rule

Then, how could the light-matter interaction be understood? From the viewpoint of matter, light is the external stimulus. Thus, it becomes apparent to deal with the interaction with the perturbation theory. Especially, because light is the temporal field function, the time-dependent perturbation theory is used. Even though the following sections deal with merely sinusoidal perturbation potential, it can be further expanded to an arbitrarily oscillating field with Fourier transformation.

2.3.1 Time-dependent perturbation theory

A general solution of the time-dependent Schrodinger equation $i\hbar\frac{\partial}{\partial t}\psi(\vec{r},\ t) = \mathscr{H}_0\psi(\vec{r},\ t)$ is given by $\psi(\vec{r},\ t) = \phi_n(\vec{r})\exp\left(-i\frac{E_n t}{\hbar}\right)$ where E_n and ϕ_n is respectively the eigenvalue and the eigenfunction of the corresponding time-independent Schrodinger equation. Then, the general solution of the time-dependent Schrodinger Equation is given by

$$\psi(\vec{r},\ t) = \sum_{n=1}^{\infty} a_n(t)\phi_n(\vec{r})\exp\left(-i\frac{E_n t}{\hbar}\right)$$

where $a_n(t)$ is the weighting factor of the nth phase. Now, consider the perturbated potential of $V(t)$ so that $\mathscr{H}_0 \to \mathscr{H}_0 + \lambda V(t)$

and consequently $i\hbar\frac{\partial}{\partial t}\psi(\vec{r},\ t) = (\mathscr{H}_0 + \lambda V(t))\psi(\vec{r},\ t)$. With the modified Hamiltonian,

$$i\hbar\frac{d}{dt}a_m(t) = \sum_{n=0}^{\infty} a_n(t)\exp\left(-i\frac{(E_n - E_m)t}{\hbar}\right)\langle\phi_m|\,\lambda V\,|\phi_n\rangle$$

Here, elucidating $a_n(t)$ is the key to solving the Schrodinger equation (*i.e.* finding the $\psi(\vec{r},\ t)$) As $a_n(t)$ can be expanded as a function of λ so that

$$a_n(t) = \sum_{j=0}^{\infty} \lambda^j a_n^{(j)}(t)$$

If the approximation is delimited to the first order,

$$i\hbar\frac{d}{dt}a_n^{(1)} = \sum_{m=0}^{\infty} a_m^{(0)}\langle\phi_m|V\,|\phi_n\rangle\exp(i\omega nt)$$

Because $a_n^{(0)}(t) = 0$,

$$a_n(t) \approx -\frac{i}{\hbar}\int_0^t \langle\phi_i|V\,|\phi_n\rangle\exp(i\omega_{ni}t)dt \tag{2.6}$$

2.3.2 Optical dipole transition and the Fermi Golden Rule

Define the position vector of the positive and the negative charges as $\vec{r_+}$ and $\vec{r_-}$, respectively. Then, the dipole moment is defined by $\vec{d} = e(\vec{r_+} - \vec{r_-}) = e\vec{r}$. Then the electric potential of an oscillating

electric field is given by

$$\begin{aligned} V &= -\vec{d}\cdot\vec{E} \\ &= -e\vec{r}\cdot(E(t)\hat{e_r}) \\ &= e\vec{r}\cdot\vec{E}_0\cos(\omega t) \\ &= \frac{e\vec{r}\cdot\vec{E}_0}{2}\left(\exp(i\omega t)+\exp(-i\omega t)\right) \\ &\equiv V_0\left(\exp(i\omega t)+\exp(-i\omega t)\right) \end{aligned} \tag{2.7}$$

Consequently, by equation 2.7,

$$\begin{aligned} \langle\phi_m|V|\phi_n\rangle &= \langle\phi_m|e\vec{r}\cdot\vec{E}_0|\phi_n\rangle\cos(\omega t) \\ &= 2(V_0)_{mn}\cos(\omega t) \end{aligned}$$

Then, by equation 2.6,

$$a_n(t;\, t\geq t_0) = -\frac{2i}{\hbar}(V_0)_{nm}\exp\left(i\frac{(\omega_{nm}-\omega)}{2}t_0\right)\frac{\sin\left(\frac{(\omega_{nm}-\omega)t_0}{2}\right)}{\omega_{nm}-\omega}$$

Therefore, the transition rate is

$$\begin{aligned} R_{i\to j} &\propto |a_m(t\geq t_0)|^2 \\ &= \frac{2\pi}{\hbar^2}|\langle j|V|i\rangle|^2 g(E_j) \end{aligned} \tag{2.8}$$

where $g(E)$ is the density of states. Physically, the Fermi Golden Rule states that an 'optical transition rate is proportional to the wavefunction integral between the two states with the electrical potential.'

Consider a polarization plate for example. Provided the metal engraving is aligned in the y-direction (*i.e.* transmission axis parallel to the x-axis), the dipole vector $\vec{d}$ is restricted to have direction only parallel to the y-axis. Then, for the x-oscillating field would render the electric perturbation potential to be 0 and hence the transition rate $R_{i\to j}$. In other words, the plate does not optically militate any effect on the x-polarized light. Contrastingly, in the case of y-polarized light, the potential would be maximized so that the light would be effectively absorbed by the metal engravings. Accordingly, the plate filters the x-polarized light.
Similarly, one can simply investigate the slab orientation distribution by using polarized light. In the case of quasi-2D perovskite, for example, the dipole vector is restricted within the 2D plane defined by the slab. Consequently, the light with its electric field oscillating in the vertical direction of the slab would not interact with the slab. Considering that only a cosine fraction of incident light would be absorbed by the slab and that each slab with different atomic thickness (*i.e.* different n) absorbs light with its characteristic absorption peak, one can obtain $\langle \theta,\ \phi \rangle (n)$ of the sample in a rather simple way.
As such, the Fermi Golden Rule, as its name states, is the initiating point of the light-matter interaction.

2.4. Jablonski Diagram

Heretofore, you have learned how light interacts with matter. The next step is to investigate what transitions are viable and their mechanism. This section provides a bird-eye view of optical transitions in real-world applications.

2.4.1 Exchange operator and the Pauli exclusion principle

Are two arbitrary electrons distinguishable? One can answer this question by shedding light on their exchange. Consider the wavefunction $\psi(1,\ 2)$ that describes two particles 1 and 2, and the exchange operator $\mathfrak{C}$ that exchanges the two particles. Then, apparently, $\mathfrak{C}$ is a Hermitian operator because

$$\begin{aligned}
\langle f|\,\mathfrak{C}\,|g\rangle &= \iint f^*(r_1,\ r_2)\mathfrak{C}g(r_1,\ r_2)dr_1dr_2 \\
&= \iint f^*(r_1,\ r_2)g(r_2,\ r_1)dr_1dr_2 \\
&= \left(\iint f(r_1,\ r_2)g^*(r_2,\ r_1)dr_1dr_2\right)^* \\
\text{(by variable exchange)} &= \left(\iint g^*(r_1,\ r_2)f(r_2,\ r_1)dr_1dr_2\right)^* \\
&= \left(\iint g^*(r_1,\ r_2)\mathfrak{C}f(r_1,\ r_2)dr_1dr_2\right)^* \\
&= \langle g|\,\mathfrak{C}\,|f\rangle^*
\end{aligned}$$

Since it is a Hermitian operator, it constitutes an eigenvalue equation of

$$\begin{aligned}
\mathfrak{C}\psi(1,\ 2) &= \psi(2,\ 1) \\
&= C\psi(1,\ 2)
\end{aligned}$$

Therefore

$$\begin{aligned}
\mathfrak{C}^2\psi(1,\ 2) &= C^2\psi(1,\ 2) \\
&= \psi(1,\ 2)
\end{aligned}$$

Consequently, the eigenvalues are ± 1. The symmetry of the wavefunction with respect to the exchange operator dictates the properties of the particle. Indeed, bosons have $C = +1$ (symmetric) and fermions have $C = -1$ (antisymmetric). This is articulated by the famous Pauli's exclusion principle.

> **Pauli's Exclusion Principle.** The total wavefunction of a system comprised of identical fermions is antisymmetric with respect to the exchange operator.

Say that the system with the two identical particles respectively at different states is described by

$$\Psi(1,\ 2) = c_1 \psi_a(1)\psi_b(2) + c_2 \psi_a(2)\psi_b(1)$$

Then, the eigenvalue of the fermion system with respect to the exchange operator has the following relationship with the coefficients.

$$c_1 = -c_2 = \frac{1}{\sqrt{2}}$$

2.4.2 Singlet and triplet

Now, take a spin into account. Then the total wavefunction of a system could be described with the multiplication of spatial wavefunction and spin wavefunction. In this case,

$$\begin{aligned} \Psi(1,\ 2) &= (c_1\phi_a(1)\phi_b(2) + c_2\phi_a(2)\phi_b(1))\, s(1,\ 2) \\ &= \Phi(1,\ 2)s(1,\ 2) \end{aligned} \tag{2.9}$$

Two make the whole wavefunction antisymmetric, (recall section 2.4.1) two following cases are feasible.

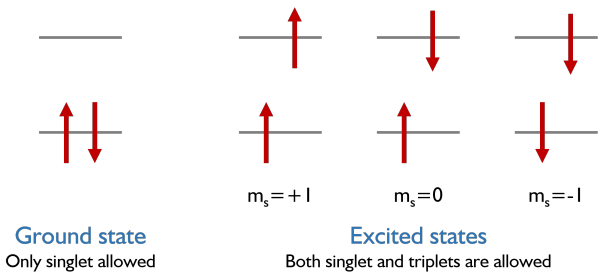

Fig. 2.2. Allowed spin states

Symmetric $\Phi(1,\ 2)$ and antisymmetric $s(1,\ 2)$

In this case, it is apparent that $c_1 = c_2 = 1/\sqrt{2}$. Then, accordingly, the spin wavefunction is restricted to have only

$$s(1,\ 2) = \frac{1}{\sqrt{2}}\left(|\uparrow\downarrow\rangle - |\downarrow\uparrow\rangle\right)$$

Because it has only one feasible spin state function, this state is called the singlet state.

Antisymmetric $\Phi(1,\ 2)$ and symmetric $s(1,\ 2)$

In this case, $s(1,\ 2)$ would have three options.

$$s(1,\ 2) = \begin{cases} |\uparrow\uparrow\rangle & (m_s = +1) \\ \frac{1}{\sqrt{2}}\left(|\uparrow\downarrow\rangle + |\downarrow\uparrow\rangle\right) & (m_s = 0) \\ |\downarrow\downarrow\rangle & (m_s = -1) \end{cases}$$

Similarly to the opposite case, $c_1 = -c_2 = 1/\sqrt{2}$. Because it has three available spin state functions, it is called the triplet state. It

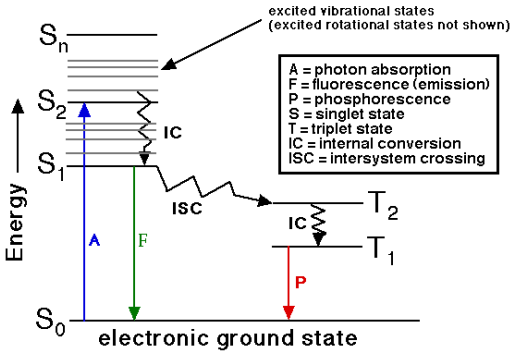

Fig. 2.3. Jablonski diagram

is noteworthy that the spatial part of the system wavefunction becomes zero if the two fermions are in the same state. Therefore, such a state is prohibited. In the case of electrons, the discussions above are summarized in figure 2.2.

2.4.3 Spin-orbit coupling, forbidden transition, and Jablonski diagram

Recall the Fermi's golden rule. (see section 2.3) Basically, it has nothing to do with spin restriction. In other words, the spin state function remains intact throughout the optical processes. Therefore, because only the singlet state is allowed in the ground state, only singlet-to-singlet transition is allowed according to Fermi's golden rule. The light emission that corresponds to the transition is called fluorescence.
Contrastively, the triplet-singlet transition is forbidden according

to Fermi's golden rule because it entails spin flipping. In reality, however, spin could be flipped. Recall that Fermi's golden rule is based on the first-order perturbation theory. Therefore, in the system where higher-order perturbation becomes notable, spin invariance may not be held. For example, a strong magnetic field enables spin flipping during optical transitions and under ambiance.
Not only the external field but also the atomic nucleus itself exerts a magnetic field on an electron. Envisage an electron revolving around the nucleus. From the electron's viewpoint, the nucleus revolves it around. The rotating charged actor itself constitutes current and the current generates a magnetic field around it. Because the magnetic flux density is proportional to the current, the higher the nuclear number the system has, the stronger the electric field the electron would sense. Therefore, in a typical inorganic semiconductor, the feasibility of spin-flipping becomes vivid. In that case, the triplet-to-singlet transition becomes salient and is called phosphorescence. Jablonski diagram depicts the optical states and relevant transitions. (see figure 2.3)

CHAPTER 3

Absorption spectra analysis

Kudos! You have got the basic toolkits for the optoelectronic analysis. From now on, you will dive into how information extracted from optical and electrical surveys could be utilized to get a deeper understanding of your materials or devices. Optical analysis is an extremely facile modality to get rich information from the sample. We will begin our journey by scrutinizing how the absorption spectrum could be the fountain of insight.

3.1. Rudimentary optics

3.1.1 Optical Admittance

Recall the Maxwell equations.

$$\begin{aligned} \nabla \cdot \mathbf{E} &= \frac{\rho}{\varepsilon} \\ \nabla \times \mathbf{E} &= -\mu \frac{\partial}{\partial t} \mathbf{H} \\ \nabla \cdot \mathbf{H} &= 0 \\ \nabla \times \mathbf{H} &= J + \varepsilon \frac{\partial}{\partial t} \mathbf{E} \end{aligned} \tag{3.1}$$

Then, the optical admittance is defined by the amplitude ratio between the magnetic field and the electric field.

$$Y \equiv \frac{|\mathbf{H}|}{|\mathbf{E}|}$$

3.1.2 Fresnel Loss

At every single juncture in the light propagation, the continuity theorem should be satisfied. As such, at every interface, the electric field and magnetic field have to be preserved. By that, the Fresnel transmission and reflection coefficients are respectively defined

by

$$
\begin{aligned}
t &= \frac{E_t}{E_i} = \frac{2Y_1^{eff}}{Y_1^{eff} + Y_2^{eff}} \\
r &= \frac{E_r}{E_i} = \frac{Y_1^{eff} - Y_2^{eff}}{Y_1^{eff} + Y_2^{eff}} \\
\text{where } \frac{Y_j^{eff}}{Y_0} &= \begin{cases} n_j & \text{(normal incidence)} \\ n_j \cos\theta_i & \text{(s-polarization)} \\ n_j / \cos\theta_i & \text{(p-polarization)} \end{cases}
\end{aligned}
\tag{3.2}
$$

Note that the coefficients must be distinguished from reflectance and transmittance. (they are defined as the ratio of intensities.) Also, from the above equation, it can be easily deduced that all the reflections at the interface with absorptive materials ultimately retards the phase.

3.1.3 Optical resonator effect

A multi-layer film constitutes Fabry-Perot resonators. For the sake of simplicity, here we stick to a single-layer resonator. For the angle θ within the layer of thickness d and refractive index n, the output intensity is proportional to

$$
f_{FP}(\lambda) = \frac{T_1 + T_2}{(1 - \sqrt{R_1 R_2})^2 + 4\sqrt{R_1 R_2} \sin\left(\frac{\phi_1 + \phi_2}{2} + \frac{2\pi n d \cos\theta}{\lambda}\right)} \tag{3.3}
$$

Consequently, the output would be maximized if the optical length of the layer makes the sine term in the denominator negative. As

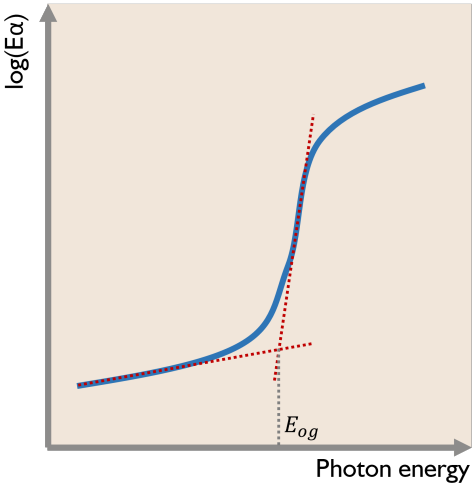

Fig. 3.1. Tauc plot

such, the resonator effect could be maximized and so is the output intensity.

3.2. Tauc plot and optical bandgap

The foremost information that could be extracted from an absorption spectrum is the bandgap of the material. From classical semiconductor physics, provided the density of states of the two bands remain parabolic, (*i.e.* conduction band and valence band have the density of state proportional to $\sqrt{\Delta E}$ near their tail) for the refractive index $n(E)$ and optical absorption $\alpha(E)$, it is widely known

that,

$$E\alpha(E)n(E) \propto (E - E_{og})^2 \tag{3.4}$$

Equation 3.4 is often called the Tauc expression. However, in real crystal, the density of states may not follow the exact parabolic dependence. In the case of quartic dependence, the famous Davis-Mott expression is obtained.

$$E\alpha(E)n(E) \propto (E - E_{og})^3 \tag{3.5}$$

For example, low-pressure CVD-deposited a-Si is well known to follow the quartic dependence and therefore is soundly fitted by the Davis-Mott expression. In general, for arbitrary crystalline materials, $E\alpha(E)n(E) \propto (E - E_{og})^n$ where n depends on the electronic structure of the material.
The relationship can be expressed in a linear form by taking logarithms to both sides. The plot is called the Tauc plot and is used to obtain the optical bandgap E_{og}. It is determined by the position at the cross point of the two extrapolation lines corresponding to the baseline and Urbach tail. (see figure 3.1)

3.3. Scattering effect

Typical thin film inherently bears optical scattering. Microscopically, it is the process of inducing a dipole oscillation within the material. Because all the atoms are thermally excited at room temperature, the spatial scattering profile is dictated by a random process with a given probabilistic density function.
Scattering efficiency Q is defined as the ratio of scattering cross-section to physical cross-section. For a spherical scatterer with its

radius r and refractive index n, the scattering efficiency is defined by the size of the scatterer relative to wavelength λ.
For large scatterer limit, where $\lambda \ll r$,

$$Q = 2$$

For the Mie scattering regime, where $\lambda \approx r$,

$$Q = 2 - \frac{4}{\rho}\sin\rho + \frac{4}{\rho^2}(1-\cos\rho)$$
$$\text{where } \rho \equiv \frac{2\pi}{\lambda}(2r(n-1))$$

For the Rayleigh scattering regime, where $\lambda \gg r$,

$$Q = \frac{128\pi^4}{3}\left(\frac{n^2-1}{n^2+2}\right)^2\left(\frac{r}{\lambda}\right)^4$$

One may wonder why the scattering efficiencies all exceed 1. But it would become apparent if you recall both geometric cross-section and diffraction contribute to the optical scattering cross-section. For example, in the large-scatterer limit, $Q_1 = 1$ is from the apparent 'shadow' of the scatterer and another $Q_2 = 1$ is from diffraction. (So that $Q = Q_1 + Q_2$)
Then, we move on to the quasi-2D perovskite analysis. As can be seen in figure 3.2, the grain size of quasi-2D perovskite remains far smaller than the incidence and emission wavelength.
Therefore, the Rayleigh scattering regime ($d \ll \lambda$) should be applied to analyze the scattering effect of the film. In the regime,

$$I = I_0 f(\theta)\Lambda d^6\left(\frac{2\pi}{\lambda}\right)^4$$

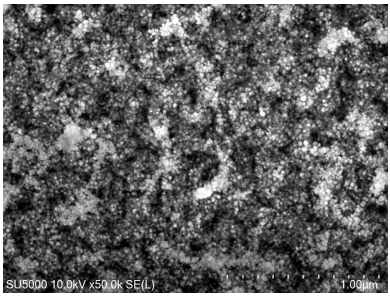

Fig. 3.2. Scanning electron microscopy image of a typical quasi-2D perovskite film

Because the transmitting-type UV-Vis spectrophotometer encompasses the scattering effect as 'absorption', (because it calculates the absorbance by $A = 1 - T$; $R = 0$) the apparent absorbance contributed by the scattering could be written by the following:

$$\begin{aligned} A_{sc} &= \log\left(\frac{I_0}{I}\right) \\ &= \Gamma_{sc} \log \lambda \end{aligned} \tag{3.6}$$

Not only the scattering effect but also Fresnel loss contributes to the apparent absorbance. Considering the configuration of the spectrophotometer, only normal incidence may be considered. There-

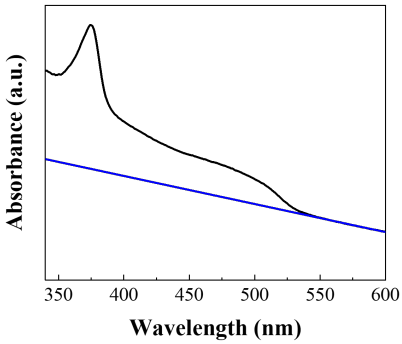

Fig. 3.3. Baseline correction in absorption spectra

fore,

$$\begin{aligned} A_{Fresnel} &= R_{Fresnel} \\ &= \left| \frac{Y_{\text{air}} - Y_{\text{PeLED, eff}}}{Y_{\text{air}} + Y_{\text{PeLED, eff}}} \right|^2 \\ &= \left| \frac{1 - (n_{\text{PeLED, eff}} + i\kappa_{\text{PeLED, eff}})}{1 + (n_{\text{PeLED, eff}} + i\kappa_{\text{PeLED, eff}})} \right|^2 \end{aligned} \tag{3.7}$$

In equation 3.7, one should note that Y_j is the optical admittance of the jth layer, and consequently potentially be a wavelength-dependent complex number. But for the sake of succinctness, we set the optical admittances to be constant. Considering equation 3.6 and 3.7, one can simply express the general baseline by:

$$A_{base} = \Gamma_{sc} \log \lambda + \Gamma_{Fresnel} \tag{3.8}$$

Practically, this can be obtained by fitting the 'clearly non-emitting' region to equation 3.8. In green-emitting quasi-2D perovskite thin film for example, it is apparent that the photoluminescence would not contribute to the signal in the region where wavelength over $550nm$. Consequently, as shown in figure 3.3, in which the blue line indicates the baseline,

3.4. Oscillator strength

As discussed earlier, an oscillation of an electric field is the result of dipole oscillation. Consider an electron density cloud displaced by x by an external electric field. Then, the equation of motion of the electron is described by

$$m_0 \frac{d^2}{dt^2} x = -kx + eE(t) - 2m_0 \gamma \frac{d}{dt} x \tag{3.9}$$

where γ is the damping constant of the system and the restoration force constant $k = m_0 \omega_0^2$. Given the sinusoidal external field of $E(t) = E(\omega)\exp(-i\omega t)$, one can simply postulate an ansatz for x to be $x(t) = x(\omega)\exp(-i\omega t)$. (Recall the rudimentary differential equation courses) Then, the equation yields

$$x(\omega) = -\frac{e}{m_0} \frac{1}{\omega^2 + 2i\gamma\omega - \omega_0^2}$$

Then, the susceptibility of the system would be given by

$$\begin{aligned}\chi(\omega) &= \frac{P(\omega)}{E(\omega)} \\ &= ne\frac{x(\omega)}{E(\omega)} \\ &= -\frac{ne^2}{2m_0\sqrt{\omega_0^2-\gamma^2}}\left(\frac{1}{\omega-\sqrt{\omega_0^2-\gamma^2}+i\gamma}-\frac{1}{\omega-\sqrt{\omega_0^2+\gamma^2}+i\gamma}\right)\end{aligned} \tag{3.10}$$

This bulk susceptibility could be also derived from the Schrodinger equation with the Coulombic potential-based Hamiltonian. Therefore, we define oscillator strength f_n by

$$\begin{aligned}\chi(\omega) &= -\frac{n}{\hbar}\sum_j e^2\left|x_{ij}\right|^2\left(\frac{1}{\omega+E_{ij}/\hbar+i\gamma}-\frac{1}{\omega-E_{ij}/\hbar+i\gamma}\right) \\ &= \frac{ne^2}{2m_0}\sum_j\left(\frac{f_{ij}}{E_{ij}}\left(\frac{1}{\omega-E_{ij}+i\gamma}-\frac{1}{\omega+E_{ij}+i\gamma}\right)\right) \\ &\text{where } f_{ij} = 2m_0\left|x_{ij}\right|^2 E_{ij} \\ &\text{and } x_{ij} = \langle i|\hat{x}|j\rangle \\ &\text{and } E_{ij} = E_i - E_j\end{aligned} \tag{3.11}$$

Then,

$$\sum_k f_{hj} = 2m_0\sum_k \langle k|\hat{x}|j\rangle\langle j|\hat{x}|k\rangle(E_k-E_j) \tag{3.12}$$

and from the original Schrodinger equation, $\mathscr{H}|k\rangle = E_k|k\rangle$,

$$\begin{aligned}
\langle j|\hat{x}|k\rangle (E_k - E_j) &= \langle j|\hat{x}E_k|k\rangle - \langle j|\hat{x}E_j|k\rangle \\
&= \langle j|\hat{x}\mathscr{H}|k\rangle - \langle k|\hat{x}E_j^*|j\rangle^* \\
&= \langle j|\hat{x}\mathscr{H}|k\rangle - \langle k|\hat{x}\mathscr{H}^*|j\rangle^* \\
&= \langle j|\hat{x}\mathscr{H}|k\rangle - \langle j|\mathscr{H}\hat{x}|k\rangle \\
&= \langle j|[\hat{x},\ \mathscr{H}]|k\rangle
\end{aligned}$$

Therefore, equation 3.12 would be

$$\begin{aligned}
\sum_k f_{hj} &= 2m_0 \langle j|\hat{x}[\mathscr{H},\ \hat{x}]|j\rangle \\
&= m_0 \langle j|[\hat{x},\ [\mathscr{H},\ \hat{x}]]|j\rangle \\
&= m_0 \left(\frac{1}{m_0}\langle j|j\rangle\right) \\
&= 1
\end{aligned} \tag{3.13}$$

Equation 3.13 is called the oscillator strength sum rule. It implies that the overall oscillator strength can be written as a linear sum of contributions from subsystems. Fundamentally, in tandem with the Maxwell equations, it constitutes the linearity of optoelectronic systems.

3.5. Elliott theory

A typical crystalline semiconductor material has two origins of its absorption: (1) continuum and (2) exciton. The Elliott theory describes how light with a given energy would be absorbed by the

material. Albeit this section would stick to the direct bandgap materials, it can be further expanded to indirect and forbidden transitions.

For electron-hole recombination in direct bandgap materials, the total momentum of the system should be 0 because $k_e = -k_h$. Consequently, the transition rate for an exciton of the nth excited state is given by:

$$A_{ex} \propto |\langle 0|\,\hat{\sigma}\,|n\rangle|^2 S_n(E) \tag{3.14}$$

where $\langle 0|\,\hat{\sigma}\,|n\rangle$ is the optical overlap between the recombination state (zero-state) and excited state and $S_n(E)$ is related to the density of states. Similarly, the continuum absorption transition rate can be expressed by simply expanding equation 3.14.

$$A_c \propto \int |\langle 0|\,\hat{\sigma}\,|n\rangle|^2 S(E)dE \tag{3.15}$$

Combining equation 3.14 and 3.15, the total absorbance is given by:

$$\begin{aligned}
\alpha(E) &= \mu^2\sqrt{E_b}\left(\alpha_c + \sum_n \alpha_{ex,\,n}\right) \\
\text{where } \alpha_c &= \int_{E_g}^{\infty} \mathfrak{H}\left(\frac{\hbar\omega - E}{\Gamma}\right) \cdot \frac{1 + b(E - E_g)}{1 - \exp\left(-2\pi\sqrt{\frac{E_b}{E - E_g}}\right)} dE \\
\alpha_{ex,\,n} &= \frac{2E_b}{n^3}\mathfrak{P}\left(\frac{\hbar\omega - E_{ex,\,n}}{\Gamma}\right)
\end{aligned} \tag{3.16}$$

where the absolute energy is defined to be 0 at the valence band maximum and $g\left(\frac{\hbar\omega - E}{\Gamma}\right)$ is the density of states considering the

spectral linewidth Γ. (A more detailed explanation of Γ is provided in section 4.2)
Note that, in equation 3.16, the Heaviside step function and excitonic peak function are respectively given by

$$\mathfrak{H}(x) = \begin{cases} 0 & (x < 0) \\ 1 & (x \geq 0) \end{cases}$$

$$\mathfrak{P}(x) = \begin{cases} \delta(x) & \text{(ideal)} \\ \frac{1}{\sqrt{2\pi}} \exp\left(-\frac{x}{2}\right)^2 & \text{(real)} \end{cases}$$

Moreover, the term $b(E - E_g)$ is a correction term for the superquadratic behavior of the conduction and valence bands near the CBM and VBM and therefore becomes negligible when it comes to halide perovskites. (Recall, from section 3.4, that spin-orbit coupling in a typical crystalline semiconductor material is irrelevant to the parabolicity of the bands.)
The Elliott theory is frequently used to estimate the exciton binding energy $E_b(T)$ as a function of temperature. In that case, temperature-dependent absorption spectra are acquired. However, the theory is a versatile tool in analyzing multi-component (ensemble) systems such as quasi-2D perovskite film, especially in performing deconvolution as shown in figure 3.4.
The appearance of the excitonic absorption peak tends to be vivid with narrower spectral linewidth Γ and larger exciton binding energy E_b. Consequently, more confined phases show more lucid peak behavior. In the case of quasi-2D perovskite film, in which a plethora of reduced-dimension perovskite phases are mixed, the

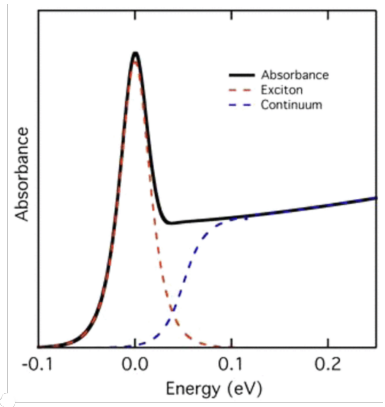

Fig. 3.4. Deconvolution of absorption spectra with the Elliott theory

Elliott theory can be used to quantitatively estimate how much amount of each phase would be in the film.

You should be extremely vigilant in assessing if a perovskite thin film is quasi-2D. Apparently, you can simply stipulate a sample quasi-2D perovskite if it exhibits excitonic peaks at the characteristic positions anticipated by the confined potential model. (see section 2.2) However, in the case of a 'smooth' absorption curve, it could be perilous to simply predicate whether it is quasi-2D or not. There are a plethora of possible reasons for ill-defined excitonic absorption peaks. Therefore, it could be concluded that quasi-2D only if there is sufficient evidence from other temporal optical modalities such as transient absorption spectroscopy (TAS). For example, if you have a 'smooth' absorption curve while the TAS spectrum shows rather broad spectral linewidth for the phase, indistinct excitonic peaks may be justified. However, in the oppo-

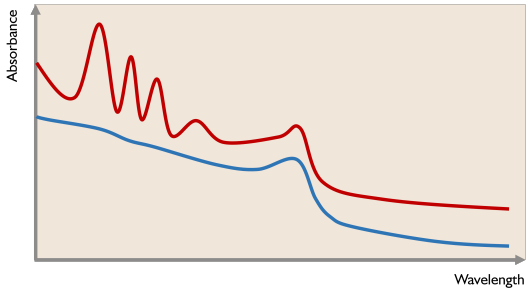

Fig. 3.5. Absorption spectra of quasi-2D perovskites

site case, you have to sentence against the sample asserting itself quasi-2D.

Here, note that not every 'peak' on an absorption spectrum may have attributed to an excitonic absorption. It might have originated from the wavelength-dependent Fresnel loss or an optical resonator effect. (Recall sections 3.1.2 and 3.1.3)

Last but not least, note that equation 3.16 is based on Bloch wavefunctions albeit equations 3.14 and 3.15 are from Fermi's golden rule. (see section 2.3 Therefore, it is only valid for crystalline structures including quantum dots and polycrystalline materials. Note that in the case of magic-sized clusters with distinct structures (*e.g.* InP magic-sized cluster), the Elliott theory may not be applied.

3.6. Ideal absorption spectra of a highly emissive quasi-2D perovskite film

Then, what would be the ideal absorption spectrum of an energy-funneled system? For efficient energy funneling, the optical spectral overlap between two adjacent phases should be maximized. Recalling section 2.3 and 3.5, it becomes apparent that having large spectral linewidth is the crucial factor in yielding a highly efficient energy funneling process. In the case of quasi-2D perovskites, for example, the linewidth of the low-n phases should be sufficiently large, and in that case, as already discussed in section 3.5, excitonic absorption peak may not be visible. In other words, the film may have a somewhat 'smooth' absorption curve in a short-wavelength regime.
However, the final emitting phase should have narrow spectral linewidth. This is acceptable because, in a large n regime, the energy gap between the two adjacent n phases would be fairly small. Therefore, the most desirable absorption spectrum would be something similar to the blue line in figure 3.5.

CHAPTER 4

Photoluminescence spectra analysis

Following absorption, photoluminescence is another important characteristic in analyzing optoelectronic materials. For example, the quantum yield itself is a dictating factor of the external quantum efficiency of a light-emitting diode. As such, it renders the overall performance of your devices. In this chapter, a quasi-classical description of light emission and its related properties are described. To this end, it would provide you with how the optical properties, including color purity and luminescence efficiency of your materials, could be modulated.

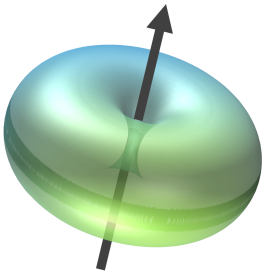

Fig. 4.1. Dipole radiation pattern

4.1. Dipole emission

Consider the harmonically oscillating dipole $p = p_0 \sin(\omega t)$. Then, the radiation fields are given by

$$\vec{E} = \frac{\sin(\theta)}{4\pi\varepsilon rc^2}\frac{d^2p}{dt^2}\hat{\theta}$$
$$\vec{B} = \frac{\mu\sin(\theta)}{4\pi rc}\frac{d^2p}{dt^2}\hat{\phi}$$

Therefore, the time-averaged angular distribution of the Poynting vector is given by

$$\langle S(\theta,\ \phi)\rangle = \frac{\mu w^2 I_0^2 d^2}{32\pi^2 c}\left(\frac{\sin^2\theta}{r^2}\right)\hat{r} \tag{4.1}$$

Equation 4.1 has a doughnut shape. One can easily deduce the total radiation pattern by simply conjugating the dipole distribution pattern with the dipole radiation pattern (equation 4.1). For example, an ideal 2D plate would generate a dumbbell-shaped radiation pattern. (See figure 4.2)

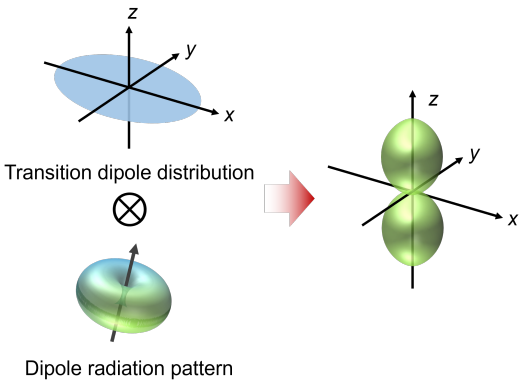

Fig. 4.2. Emission pattern of a 2D nanoplatelet

However, in the case of real quasi-2D materials, a little tolerance of transition dipole in z-direction is allowed. In other words, the transition dipole distribution would no longer remain in the $x-y$ plane but would have a somewhat 'plate with thickness' form. In that case, because of the z-component of the convoluted function, the dumbbell would be shrunk in the z-direction while being broadened in the radial direction. As such, 0D quantum dots and 1D nanorods would have isotropic (yet not spherical) and doughnut-shaped radiation patterns, respectively.

4.2. Temperature-dependent emission profile

The emission linewidth of a material is governed by phonon interaction. For the majority of inorganic materials and perovskites, the

spectral linewidth is given by

$$\Gamma(T) = \Gamma_0 + \Gamma_{ac}T + \frac{\Gamma_{LO}}{\exp\left(\frac{E_{LO}}{kT}\right) - 1} + \Gamma_{imp}\exp\left(-\frac{E_b}{kT}\right) \quad (4.2)$$

where Γ_0 is the inhomogeneous broadening factor and Γ_{ac} term describes the homogeneous broadening by acoustic phonon scattering. The Γ_{ac} is the acoustic phonon-exciton coupling strength. Moreover, Γ_{LO} is the coupling strength of the interaction between a longitudinal optical phonon and an exciton. It is also a part of the homogeneous broadening. Last but not least, the final term describes the linewidth broadening by impurities. It follows a typical Arrhenius-type dissociation pattern. Even though equation 4.2 has some limitations including the temperature-independent phonon energy assumption, which is not true in typical reduced-dimension materials.

The apparent rotational degree of freedom of an ion in a crystalline material may broaden the spectral linewidth of the material. Therefore, cesium-based perovskite tends to have a narrower FWHM compared to methylammonium or formamidinium-based crystals, because a cesium ion in the A-site has a spherical symmetry. Likewise, formamidinium-doped methylammonium-based perovskites have a narrower spectral linewidth compared to those with pure methylammonium. Methylammonium in typical halide perovskites exhibits dipolar relaxation behavior, the rotational relaxation of the methylammonium ion within the A-site after the external field removal, and the addition of formamidinium impedes the relaxation by increasing the corresponding activation energy. (see figure 4.3) Therefore, it would be imperative to mix formamidinium if you opt for methylammonium as a constituent of the

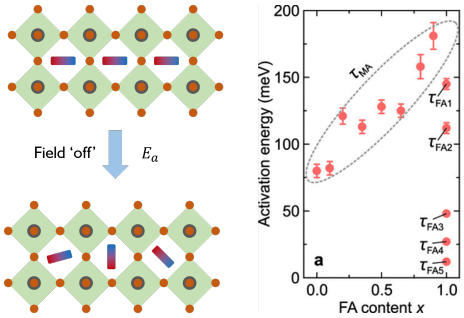

Fig. 4.3. Dipolar relaxation of A-site cation in $MA_{1-x}FA_xPbBr_3$

A-site cations of halide perovskites.

One should remember that not every phase should have narrow Γ in energy-funneled systems. In that case, it is the phase with the smallest bandgap that dictates the total emission characteristics. For example, broad emission profiles of the small-*n* phases may be beneficial, or even imperative, to yield highly emissive quasi-2D films. (See section 3.6) Rather, it is important to maintain a narrow linewidth of the terminal light-emitting phases.

The spectral linewidth may be broadened by the distortion of the perovskite lattice. Along with the growing deviation from the robust and rigid lattice, it becomes more susceptible to the phonon interaction. Accordingly, it tends to have a broader emission linewidth. For example, in the case of ⟨110⟩-truncated 2D phases, well known to have large deviance from the well-defined rectangular lattice, exhibits very broad emission bandwidth because of both large exciton-phonon interaction as well as self-trapped exciton behavior (see section 4.3), and is often used for white light-emitting applications

accordingly. Its lattice susceptibility is attributed to additional hydrogen bonding between the spacer molecules and the lead halide polyhedron.

Similarly, one cannot achieve a narrow emission profile with a chiral nanomaterial. The chirality of a nanomaterial has two origins. Firstly, chiral organic additives give the 'composite' chirality. It is the simplest way to fabricate 'chiral nanomaterials' but its properties other than optical characteristics do not deviate from the original materials. Contrastingly, chirality could be transferred from the organic ligand to the crystal by distorting the lattice. In this case, the circular dichroism pattern would be different from that of the chiral ligand. (*i.e.* new peaks appear or the intensities of some peaks are undermined) It is lucidly highlighted in many fields because it has distinctive and special properties compared to achiral materials. However, from the optical viewpoint, it cannot generate spectrally narrow light because of its distorted (and hence metastable) lattice geometry. As such, it is physically impossible to achieve narrow spectral linewidth and saliently efficacious chirality transfer simultaneously.

It is the Huang-Rhys factor S that dominates the bandgap of the material. Given the average phonon energy $\langle E_{ph} \rangle$, temperature-dependent bandgap energy is articulated by

$$E_g(T) = E_g(T=0) + S\langle E_{ph} \rangle \left(\coth \left(\frac{\langle E_{ph} \rangle}{2kT} \right) - 1 \right) \tag{4.3}$$

Similarly, emission spectral linewidth is stipulated by the Huang-Rhys factor following the bandgap as

$$\text{FWHM} = 2.36\sqrt{S}\langle E_{ph} \rangle \sqrt{\coth \left(\frac{\langle E_{ph} \rangle}{2kT} \right)} \tag{4.4}$$

You can find the Huang-Rhys factor S of the materials in many related articles.
As shown in equation 4.2, 4.3, and 4.4, both bandgap and linewidth of material tend to increase as a function of temperature unless any significant phase transition occurs.

4.3. Self-trapped exciton

The discussions heretofore have assumed that the lattice is robust and is not affected by the localization of a charge carrier. However, in reality, the localization of an exciton may change the free energy landscape of the lattice geometry. For example, in a typical 2D perovskite, localization of exciton distorts the lattice geometry and stabilizes the exciton energy than its original state dictated by the 'fixed lattice' assumption. Such a new recombination channel is called the self-trapped exciton. (see the corresponding Jablonski diagram in figure 4.4)
The competition between the normal exciton and self-trapped exciton is governed by the thermal activation process and hence Arrhenius formalism. Self-trapped exciton inevitably broadens emission linewidth in a bathochromic way because it adds more stable recombination channels. Moreover, it tends to have a very large Stokes shift compared to typical 3D perovskites. In other words, the Huang-Rhys factor of the system (see equation 4.4) has a positive correlation with the self-trapped exciton emission. Therefore, in the field of white light emission, it is the foremost and imperative requirement to have an efficient self-trapped exciton channel. (*i.e.* higher S) However, the overly large S may lead to efficient phonon emission and ultimately increase the non-radiative recom-

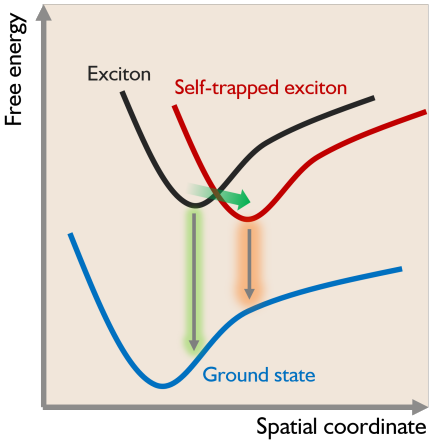

Fig. 4.4. Self-trapped exciton

bination rate. As such, maintaining a fair level of the Huang-Rhys factor is crucial in achieving both fair quantum yield and broadband emission.

In the field of perovskite, reduced-dimension perovskites are known to have a salient degree of self-trapped exciton generation owing to their structural susceptibility and distortion. Quantitatively, the deviation of the bond length and bond angle from the equilibrium of the rigid crystal defines the structural susceptibility. The two

factors are defined by

$$\Delta d = \frac{1}{n} \sum_{j=1}^{n} \frac{(d_j - d_0)^2}{d_0}$$
$$\sigma^2 = \frac{1}{11} \sum_{j=1}^{12} (\theta_j - 90)^2 \tag{4.5}$$

It is to endow an appropriate S to the system why prominent examples opt to adopt alkylammoniums which secure at least the minimal degree of rigidity of the crystals.

CHAPTER 5

Electrical Analysis

Heretofore, you have dealt with optical methods to scrutinize the material. In this chapter, you will encounter how electrical parameters can be versatile modalities in analyzing not only materials but also the whole device. Starting with the diode equation, this chapter covers the $J-V$ curve characteristics and is finalized with the recombination zone. Throughout the chapter, a steady-state flow of charge carriers is assumed. To this end, provided a fundamental basis in electrodynamics, this chapter provides you with the last snippet of optoelectronic analysis of light-emitting materials and devices.

5.1. Diode equation

The Shockley diode equation states that

$$J = J_0 \left[\exp\left(\frac{eV}{\eta kT} \right) - 1 \right] \tag{5.1}$$

For layered structure, one can define voltage V_i and current density J_i for each layer respectively.

$$\begin{aligned} V_{tot} &= \sum V_i \\ \forall i,\ J_{tot} &= J_i \end{aligned}$$

Then, each layer would possess respective ideality factor η_i such that

$$\begin{aligned} J_{tot} &= J_0 \left[\exp\left(\frac{eV_{tot}}{\eta_{tot} kT} \right) - 1 \right] \\ &= J_0 \left[\exp\left(\frac{eV_i}{\eta_i kT} \right) - 1 \right] \ (\forall i) \end{aligned}$$

Therefore,

$$\eta_{tot} = \frac{\sum V_i}{V_j} \eta_j \tag{5.2}$$

One should note that the ideality factor of a device can be extracted by

$$\eta = \left(\frac{kT}{e} \frac{\partial}{\partial V} \ln J \right)^{-1} \tag{5.3}$$

Typically, $\eta(V)$ shows a U-shaped curve. The ideality factor of a system is dictated by $\min(\eta(V))$. For example, the ideality factor of the system shown in figure 5.1 is ~ 2.5.

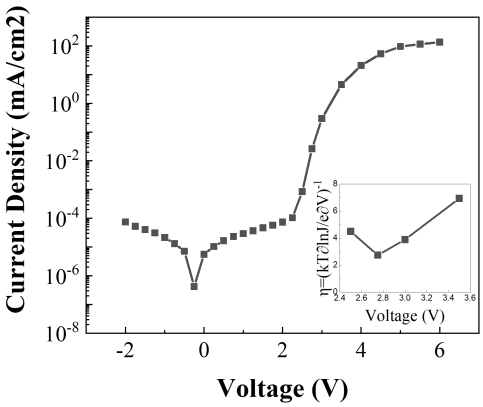

Fig. 5.1. Ideality factor $\eta = \left(\frac{kT}{e}\frac{\partial}{\partial V}\ln J\right)^{-1}$ calculation

5.2. Charge injection

A light-emitting diode is essentially an electroluminescent device. Thus, the exciton generation mechanism is radically different from photoluminescence and depends on the charge injection. Envisage an imbalanced injection of electrons and holes. It may lead to not only inefficient exciton generation but also efficient Auger processes and hence ultimately delimits the efficiency (rigorously, external quantum efficiency) of a light-emitting diode. Pragmatically, the balance of charge carrier injection is an important factor dictating the efficiency. The following parts cover how charge carriers are injected in steady-state and how electrical information can be exploited to produce imperative information on not only emis-

sion later but also interfaces.

5.2.1 Charge injection mechanism

Consider charge-carrier injection through the layer of interest. Injection of charge from another layer could be modeled with typical tunneling because the field would lower the energy of the terminal side of carrier injection (injection layer-layer of interest interface) and the potential barrier gets thinner as a stronger field is applied accordingly.
There are two major models to describe the field-induced carrier injection through a layer. The Fowler-Nordheim tunneling neglects the image charge potential by the external field while the Richardson-Schottky thermionic emission takes that into account. In the case of light-emitting diodes, in which electrons and holes are steadily and concomitantly injected into the emission layer, the image charge effect would be pragmatically neglected and hence the Fowler-Nordheim tunneling model is used to estimate the charge injection.
Under the field, the potential of the injecting layer would be described by

$$V(x) = \phi_B - eFx$$

where F is the uniform field throughout the layer and ϕ_B is the zero-field energy barrier. (see figure 5.2) Then, for the barrier width $x_0 \equiv \frac{\phi_B}{eF}$ and effective mass of the carrier m^*, the tunneling

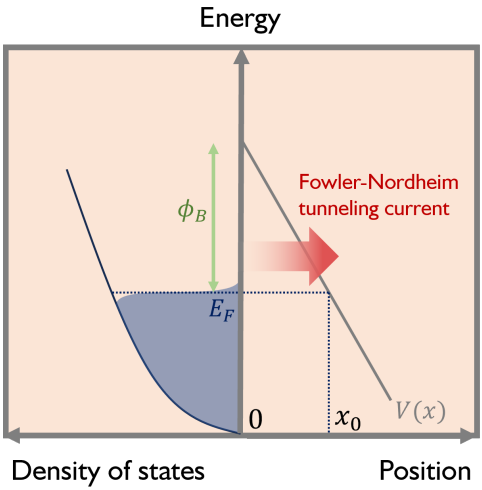

Fig. 5.2. Fowler-Nordheim tunneling

probability is given by

$$
\begin{aligned}
t &= \exp\left(-\frac{2}{\hbar}\int_0^{x_0}\sqrt{2m^*V(x)}dx\right) \\
&= \exp\left(-\frac{4}{3e\hbar F}\sqrt{2m^*}\phi_B^{3/2}\right)
\end{aligned}
$$

Thus, the Fowler-Nordheim tunneling current is given by

$$
\begin{aligned}
J_{FN} &= A^*\frac{e^2F^2}{\phi_B\alpha^2k^2}\exp\left(-\frac{2\alpha\phi_B^{3/2}}{3eF}\right) \\
\text{where } \alpha &\equiv \frac{2\sqrt{2m^*}}{\hbar} \\
\text{with the Richardson constant } A^* &= \frac{em^*k}{2\pi^2\hbar^3}
\end{aligned}
\tag{5.4}
$$

Therefore, thickening a charge injection layer would greatly reduce the current by the carrier.

5.2.2 Charge carrier injection barrier: band offset effect

It is the discrete multilayer scheme that renders the electrical behaviors of light-emitting diodes intriguing. The energy level offset often plays a critical role in the electrical behavior of a device because it ultimately dictates the steady-state charge injection dynamics.

At first, the larger the total band offset, the more retarded turn-on of the diode would be observed. Therefore, the construction of a smooth energy-level landscape throughout the device is imperative

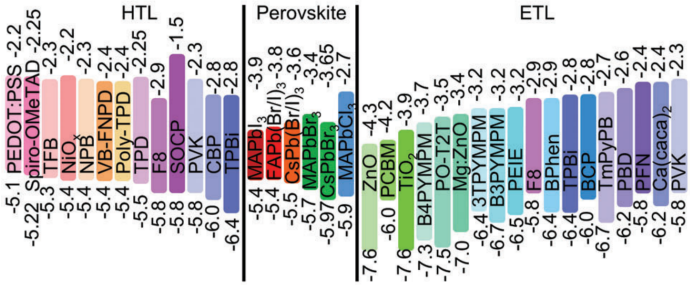

Fig. 5.3. Energy levels of materials in PeLEDs
(Adv. Electron. Mater. 2023, 9, 2201271)

to realize low-turnon voltage devices. Band extrema energies of typical materials are listed in figure 5.3.

Secondly, asymmetric band offsets for electrons and holes may result in an imbalanced carrier injection. (Recall equation 5.4) In that case, you will see a non-abrupt increase in current density in a $J-V$ plot. For example, as shown in figure 5.4, imbalanced energy level offset exhibits the 'bump' at the pre-turn-on regime. (Now, see figure 5.1. Is the $J-V$ curve exemplary?) Such asymmetry could be resolved by introducing an aligned dipole at the interface, self-assembled monolayers, for example, thereby forming local permanent polarization.

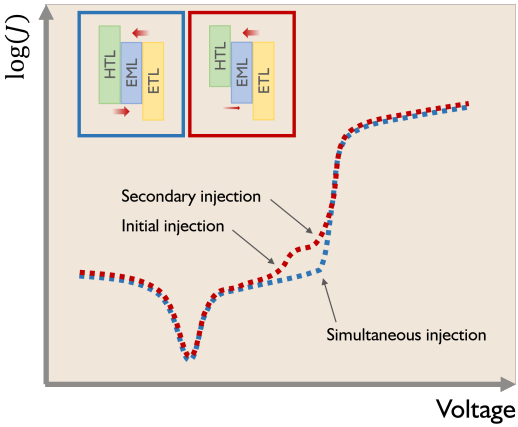

Fig. 5.4. Energy level offset and $J-V$ curve

5.2.3 Space-charge-limited current

Poole-Frenkel-like dependence

The Gauss' Law, in differential form, states that $\nabla \cdot \vec{D} = \rho(x) = en(x)$, where $\vec{D}$, $\rho(x)$, e, and $n(x)$ are electric flux density, charge density, electric charge, and carrier number density, respectively. Hence, it can be written in 1D as follows:

$$\frac{d\vec{D}}{dx} = \varepsilon \frac{d\vec{E}}{dx} = en(x) \tag{5.5}$$

The classical model of electric conduction also states that $\vec{J} = n(x)e\mu(\vec{E})\vec{E}$, where $\vec{J}$, μ, and $\vec{E}$ are current density, carrier mobility, and electric field, respectively. Combining the equation above with equation 5.5, it can be easily obtained that

$$\frac{d\vec{E}}{dx} = \frac{\vec{J}}{\varepsilon\mu(\vec{E})\vec{E}}$$

Hence, when assuming 1D for succinctness, thereby considering all the vectors as scalars, the following is obtained.

$$dx = \frac{1}{J}\varepsilon\mu(E)EdE \tag{5.6}$$

Here, we set the field dependence of mobility to be

$$\mu(E) = \mu_0 \exp(\gamma\sqrt{|E|}) \tag{5.7}$$

Combination followed by integration of equation 5.6 and 5.7 give

$$\begin{aligned} d &= \int_0^d dx \\ &= \int_{E(0)}^{E(d)} \frac{\varepsilon\mu_0 \exp(\gamma\sqrt{|E|})E}{J} dE \\ &= \frac{\varepsilon\mu_0}{J} \int_0^{E(d)} \exp(\gamma\sqrt{E})EdE \end{aligned} \tag{5.8}$$

To write it succinctly, one can define a variable $\eta = \gamma^2 E$ and a constant $\eta_d = \gamma^2 E(d)$, so that $dE = \frac{1}{\gamma^2} d\eta$. In such case, equation (5.8) would be

$$d = \frac{\varepsilon\mu_0}{J\gamma^4} \int_0^{\eta_d} \exp(\sqrt{|\eta|})\eta d\eta$$

By defining normalized current density $j = J/J_0$, where $J_0 = \frac{\varepsilon\mu_0}{d\gamma^4}$, an important equation on the normalized current density can be obtained as

$$j = \int_0^{\eta_d} \exp(\sqrt{|\eta|})\eta d\eta$$

As for voltage, one should integrate the field spatially. So the voltage can be written by

$$V = \int_0^d E(x)dx \tag{5.9}$$

By inserting equation 5.6 and 5.7 into equation 5.9, the following is obtained.

$$V = \frac{\varepsilon\mu_0}{J} \int_0^{E(d)} \exp(\gamma\sqrt{|E|})E^2 dE \tag{5.10}$$

Akin to the current density case, we can define a constant $V_0 = d/\gamma^2$. Then, equation 5.10 can be written as following:

$$\begin{aligned} V &= \frac{\varepsilon\mu_0}{d\gamma^4} \frac{d}{\gamma^2} \frac{1}{J} \int_0^{\eta_d} \exp(\sqrt{|\eta|})\eta^2 d\eta \\ &= \frac{1}{j} V_0 \int_0^{\eta_d} \exp(\sqrt{|\eta|})\eta^2 d\eta \end{aligned} \tag{5.11}$$

Defining the normalized voltage $v = V/V_0$ yields:

$$v = \frac{1}{j} \int_0^{\eta_d} \exp(\sqrt{|\eta|})\eta^2 d\eta$$

The dependence coincides with the expected results from the Poole-Frenkel mechanism. However, in the case of organic and perovskite light-emitting diodes, where energetic disorder arises owing to randomly oriented and located dipole moment, it also follows the dependence yet the exact mechanism deviates from the Poole-Frenkel mechanism.

Mott-Gurney Law

The famous Mott-Gurney law postulates that mobility is not a function of the field E. ($\mu(E) = \mu_0$) In that case, equation 5.8 would be modified as

$$\begin{aligned} d &= \int_0^d dx \\ &= \int_{E(0)}^{E(d)} \frac{\varepsilon\mu_0 E}{J} dE \\ &= \frac{\varepsilon\mu_0}{2J}(E_d)^2 \end{aligned}$$

Therefore, $E_d = \sqrt{\frac{2Jd}{\varepsilon\mu_0}}$. Likewise, equation 5.11 would be modified as follows:

$$\begin{aligned} V &= \int_0^d E(x)dx \\ &= \int_{E(0)}^{E(d)} \frac{\varepsilon\mu_0 E^2}{J} dE \\ &= \frac{\varepsilon\mu_0}{3J}(E_d)^3 \end{aligned}$$

Merging the two equations above yields

$$J = \frac{9}{8}\varepsilon\mu_0 \frac{V^2}{d^3}$$

From $\gamma^2 = d/V_0$ by the definition of V_0, one can write

$$\begin{aligned} J_0 &= \frac{\varepsilon\mu_0}{d\gamma^4} \\ &= \frac{\varepsilon\mu_0}{d}\left(\frac{V_0}{d}\right)^2 \\ &= \varepsilon\mu_0\frac{V_0^2}{d^3} \end{aligned}$$

Hence, the normalized current density $j = J/J_0$ for the case of field-independent mobility, from the aforementioned definition of the normalized voltage $v = V/V_0$, the following equation is obtained.

$$j_{M-G} = \frac{9}{8}v^2$$

5.3. Recombination zone

According to the Langevin theory, the electron-hole recombination rate γ_{eh} is given by the geometry of your device. Consider an emission layer with the thickness of d and emission zone width of w with the charge carrier travel distances of d_e and d_h for electron and hole, respectively. Along the spatial coordinate, the charge carrier densities are given by $n_e(x)$ and $n_h(x)$ likewise. As to the Langevin theory, the recombination rate is given by

$$\gamma_{eh} \simeq \frac{1}{1+\frac{w}{d}}$$

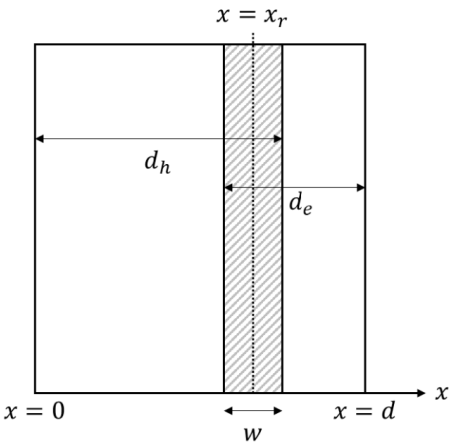

Fig. 5.5. Geometry of recombination zone and emission layer

The total 'measured' current is apparently comprised of the contribution of electrons and holes and by the definition of the current,

$$\begin{aligned} J &= j_e + j_h \\ &= eE\left(\mu_e n_e(x) + \mu_h n_h(x)\right) \end{aligned}$$

Then considering the electron-hole recombination rate γ_{eh},

$$\begin{aligned} \frac{d}{dx} j_e &= e\mu_h \frac{d}{dx} n_e(x) \\ &= -e\gamma_{eh} n_e(x) n_h(x) \\ \frac{d}{dx} j_h &= e\mu_h \frac{d}{dx} n_h(x) \\ &= -e\gamma_{eh} n_e(x) n_h(x) \end{aligned} \tag{5.12}$$

You should be able to envisage that the solution of equation 5.12 would be an exponential decay curve by intuition. (If you are not, you may have to rush into the library) For the solution given by

$$n_e(x) = n_{e,\,0} \exp\left(-\frac{d-x}{d_e}\right)$$
$$n_h(x) = n_{h,\,0} \exp\left(-\frac{x}{d_h}\right)$$

the recombination zone width in the space-charge-limited current regime is

$$\begin{aligned} w &= d_e + d_h - d \\ &= \frac{2\mu_e\mu_h}{(\mu_e+\mu_h)^2} d \end{aligned} \tag{5.13}$$

Moreover, the center position of the recombination zone is given by

$$x_r = \left(d + \frac{w}{2}\right)\left(\frac{\mu_h}{\mu_e+\mu_h}\right) \tag{5.14}$$

It is imperative to make $x_r \to \frac{d}{2}$ to avoid any potential undermining of the radiative emission efficiency due to effective Auger recombination. (note that, for example, if $x_r \leq d \leq d_h$, the hole accumulation zone and the recombination zone would be severely overlapped.)
One may alter the recombination zone position x_r by changing the relative thickness of charge transport layers. Obviously, the recombination zone would be spatially biased toward the hole injection layer if the layer becomes thicker.

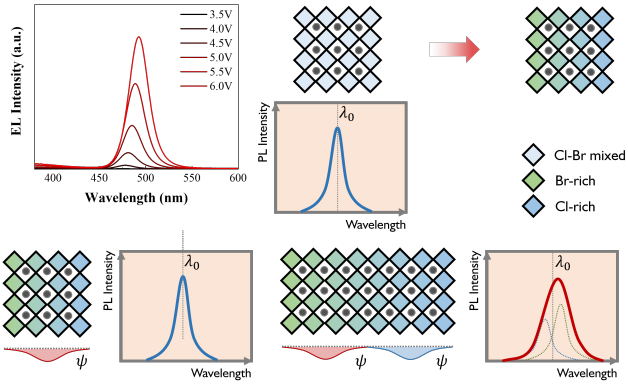

Fig. 5.6. Halide segregation in X-alloyed perovskites

5.4. Halide segregation in perovskites

In mixed halide perovskite, halide ions are segregated by external stimuli such as light illumination and electric field application. In tandem with the quantum confined Stark effect, (see section 2.2.1) the halide migration may induce typical redshift with increasing voltage applied to your device, as shown in figure 5.6.
For example, in Br-Cl alloyed perovskites, an excited state within the Cl-rich regime could be effectively transferred to its counterpart. However, you should be meticulous because not all halide segregation induces a redshift of the luminescence of the film. If the halide segregation within the region cannot be effectively 'resolved' by the excitonic wavefunction, it would emit as if it has not undergone any halide segregation. The redshift in emission appears only if the halide segregation spans in a spatially resolv-

able order. Therefore, in a typical quasi-2D film, intra-phase has virtually no effect on its emission peak wavelength and only inter-phase halide segregation militates the excitonic emission profile. In the case of quantum dots with a salient level of quantum confinement, likewise, halide segregation within the crystal may not affect the color. Consequently, light-emitting diodes with a quantum dot monolayer do not show significant redshift with respect to strengthening electric field (applied voltage). Despite excellent spectral stability upon electroluminescence operation, the advantage however would be compensated by low external quantum efficiency because of the inevitable overlap between the charge accumulation zone and recombination zone. (see section 5.3)

HANDBOOK OF OPTOELECTRONIC ANALYSIS OF LIGHT-EMITTING MATERIALS AND DEVICES

MINJAE KIM

Optoelectronics study is an assorted gift set. Spanning a plethora of disciplines, including quantum mechanics, optics, and electrodynamics, just to name a few, one in the field should be acquainted with the subjects. HANDBOOK OF OPTOELECTRONIC ANALYSIS OF LIGHT-EMITTING MATERIALS AND DEVICES provides readers with a rudimentary toolkit required for engaging with studies utilizing light-matter interactions.

The electronic version of this book is also available at
`https://mj3259.github.io`